IEEE Access
Multidisciplinary | Rapid Review | Open Access Journal

Received January 6, 2018, accepted January 30, 2018, date of publication February 9, 2018, date of current version March 16, 2018.

Digital Object Identifier 10.1109/ACCESS.2018.2804380

Impact of Data Quality in Home Energy Management System on Distribution System State Estimation

JEONG-WON KANG[1], (Student Member, IEEE), LE XIE[2], (Senior Member, IEEE), AND DAE-HYUN CHOI[1], (Member, IEEE)

[1]School of Electrical and Electronics Engineering, Chung-Ang University, Seoul 156-756, South Korea
[2]Department of Electrical and Computer Engineering, Texas A&M University, College Station, TX 77843, USA

Corresponding author: Dae-Hyun Choi (dhchoi@cau.ac.kr)

This work was supported in part by the Korea Electric Power Corporation under Grant R17XA05-75, in part by the National Research Foundation of Korea Grant through the Korea Government (MSIP) under Grant 2015R1C1A1A01051890, and in part by the National Science Foundation under Grant IIS-1636772 and Grant ECCS-1150944.

ABSTRACT As the coupling between home energy management system (HEMS) and distribution system state estimation (DSSE) becomes stronger for smart distribution grid operations, unexpected HEMS data change can, through the distortion of the HEMS solution, deteriorate the DSSE performance. In this paper, we investigate the impact of data changes in the HEMS for multiple homes on three-phase unbalanced DSSE. We develop a two-level sensitivity analysis framework based on the perturbed Karush–Kuhn–Tucker conditions from the HEMS and DSSE optimization formulations. The developed framework is used to assess the impact of the HEMS data changes in a low-voltage (LV) distribution network (at the first level) on the DSSE solutions in a medium-voltage (MV) distribution network (at the second level). Using the sensitivity framework, system operators can quantify the sensitivity of DSSE to changes in various types of HEMS data (e.g., demand response signals, appliance parameters, and consumer comfort). Along with the HEMS data impact analysis, the proposed sensitivity approach is tested under different measurement redundancy for DSSE in an IEEE 13-bus MV distribution system with 12 smart households in a radial LV network.

INDEX TERMS Distribution system state estimation, home energy management system, data change, sensitivity analysis.

I. INTRODUCTION

The distribution management system (DMS) [1] and the home energy management system (HEMS) [2] are essential tools for distribution system operators (DSOs) and residential load aggregators (RLAs) to conduct an efficient energy management in medium voltage (MV) and low voltage (LV) distribution networks, respectively. While the coupling between the DMS and the HEMS is further strengthened for the reliable operation of an entire MV/LV distribution network, an incorrect HEMS solution due to data changes from inherent and/or cyber threats can lead to the malfunction of the major DMS applications. The main objective of this paper is the study of the impact of HEMS data changes on the distribution system state estimation (DSSE) that is one of the key DMS applications.

Under various demand response (DR) programs and dynamic electricity tariffs (e.g., time of use (TOU) rate, real-time pricing (RTP)), HEMS is a key technology for an efficient management of the residential energy in smart grid. The HEMS monitors the real-time energy usage of consumers using a smart meter and schedules the optimal energy consumption of their home appliances along with distributed energy resources (DERs) such as rooftop solar panels and the energy storage system (ESS). A core HEMS technology is the optimization method for load reduction and load shifting. In [3], a stochastic load scheduling method for which the uncertainties from home appliance operation times and renewable energy resources are considered was proposed using linear programming (LP). Stochastic control and optimization methods were used to build a robust HEMS in [4]–[6]. The optimization of the heating, ventilation, and air-conditioning (HVAC) scheduling was developed along with electric vehicle (EV) [7]. In [8], the various types of demand side management that are potentially integrated with

HEMS were introduced. The more recent papers [9] and [10] proposed a load management method for multiple consumers for which a mixed-integer linear programming (MILP) is applied. A chance constrained optimization-based model for HEMS was proposed to resolve uncertainties that result from forecasted errors of electricity prices and loads in [11]. Various optimization formulations are summarized in [12].

Traditionally, the DMS with a limited system observability to the LV network manages and controls only the MV load. Recently, the HEMS functionality at the LV level has been extended to support the DMS at the MV level by forecasting the uncertain aggregated residential loads that are due to DERs and various demand side management (DSM) programs. In future smart grids with more diverse residential demands and unpredicted DERs, the DMS becomes increasingly dependent on the HEMS for an accurate load forecasting and efficient load management in the LV network.

It should be noted that the performance of the optimization-based HEMS highly relies on the accuracy of various types of data (e.g., smart meter energy consumption, weather forecasts, the operational parameters for appliances, consumer-preferred indoor temperatures, and the DR signals with a demand reduction request and duration). Therefore, a small change in the HEMS data may result in a significant distortion of the HEMS solution. For example, a recent paper [13] has addressed the possibility of data manipulation-based cyber attacks against the HEMS and quantified their detrimental impacts on the HEMS. Furthermore, as the coupling between the HEMS and the DMS becomes stronger for smart distribution grid operations, it is obvious that the changes in the HEMS data due to natural errors and/or cyber data attacks could lead to the malfunction of the HEMS, which in turn deteriorates the performances of the DMS applications.

In this paper, we propose a new analytical framework to quantify the sensitivity of the distribution system state estimation (DSSE) in the DMS with respect to HEMS data changes in an entire MV/LV distribution network. As an entry point in the DMS, the DSSE is a key function for the real-time monitoring of the distribution systems. The DSSE processes sensor measurements from a supervisory control and data acquisition (SCADA) system, and provides the initial operation conditions to the other DMS applications such as contingency analysis, load flow analysis, and volt-var control. Since the pioneering works of [14] and [15] regarding the three-phase DSSE, a considerable amount of literature has been published on the development of advanced DSSE methods including a linearized DSSE with a phasor measurement unit (PMU) [16], a meter placement algorithm for the determining of the optimal locations of the PMUs and smart meters [17], [18], artificial neural network (ANN)-based pseudo measurement modeling [19], new DSSE formulations for which the distributed generation (DG) and the LV load are incorporated as state variables [20], [21]. More recently, robust measurement placement methods for distribution system state estimation were developed considering network reconfiguration with the uncertainties of distributed generation output [22] and formulating the measurement placement problem using a mixed-integer semidefinite programming with distributed energy resources and volatile loads [23]. In [24], multi-area state estimation in distribution systems was presented, which calculates the estimation solution efficiently and accurately with minimum communication costs among local areas. A detailed literature review on the DSSE is given in [25].

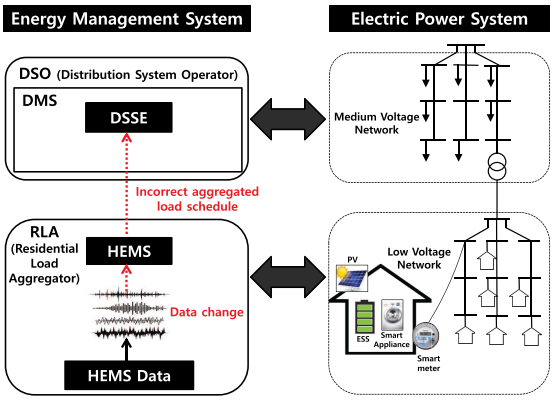

FIGURE 1. Illustration of information flow from HEMS to DSSE in the MV and LV networks.

Fig. 1 illustrates the information flow from HEMS to DSSE in the MV/LV networks when the HEMS data change. The changed HEMS data yields incorrect aggregated load schedule through the HEMS, consequently leading to the miscalculation of the DSSE solution. In this figure, the aggregated residential load from the HEMS is a key variable in our proposed sensitivity framework, connecting the sensitivities of the HEMS and the DSSE to changes in the HEMS data and in SCADA measurements, respectively. For the desired sensitivity analysis, the aggregated residential load is assumed to be a real power injection measurement at the corresponding MV bus for the DSSE.

Recent studies have shown sensitivity approach for power system applications regarding data changes. Castillo *et al.* [26] developed a general sensitivity analysis framework for the impact analysis regarding the sensitivity of nonlinear optimization subjects to data changes by perturbing the KKT conditions. This sensitivity framework has been used to assess the impact of data changes, as follows: i) locational marginal price (LMP) [27], ii) state estimation in transmission system [28], and iii) security constrained economic dispatch (SCED) [29], and iii) HEMS optimization algorithm for a house [30]. More recently, based on the results from [26] and [28], the method for quantifying the impact of multiple perturbations in data on transmission system state estimation was proposed where data that are influential to state estimation solution are identified using principal component analysis (PCA) technique [31].

However, none of the previous works have investigated the impact of HEMS data changes on the DSSE performance in *the entire MV/LV distribution network* considering:

(1) the *multiple homes* with energy trade among consumers; and (2) the *three-phase unbalanced distribution systems*. It is noted that previous studies [28], [30], [31] were limited to the sensitivity analysis of only transmission system state estimation and the HEMS for only one house regarding data changes..

The main contributions of this paper are summarized as follows:

- A sensitivity analysis framework where the impact of data changes in the HEMS for multiple houses on the DSSE can be analyzed is provided. In the LV and MV distribution networks, the interactions between multi-spatial components such as: 1) the HEMS data; 2) the aggregate scheduled residential load from the HEMS; 3) the real power injection measurement for the DSSE; and 4) the optimal solution of the DSSE (i.e., the estimated states and the objective function) are considered for the proposed framework.
- A two-level sensitivity matrix associated with the HEMS at the first level and the DSSE at the second level is derived. Each sensitivity matrix is derived using the perturbed KKT equations of its own optimization problem. The matrix that is calculated through the multiplication of two sensitivity matrices enables system operators to assess the sensitivity of the DSSE to changes in the various types of HEMS data such as DR signal, operation parameters of appliances, and consumer comfort. Numerical examples are illustrated in the IEEE 13-bus MV distribution system with 12 smart households in a radial LV network considering different measurement redundancy for DSSE.

The rest of this paper is organized as follows. Section II introduces the optimization formulation of the HEMS and the DSSE. Section III presents the proposed sensitivity matrix based on the KKT conditions perturbation approach, which is used to assess the impact of the distorted HEMS load aggregation due to data changes on the DSSE. The simulation results for the proposed sensitivity approach are provided in Section IV, and the conclusion is given in Section V.

II. BACKGROUND

The notations used in this paper are summarized in Table 1. For simplicity, the subscript p for phase is omitted in the HEMS optimization formulation.

A. HOME ENERGY MANAGEMENT SYSTEM

For each consumer $u \in \mathcal{U} := \{1, \ldots, U\}$ and the scheduling period $t \in \mathcal{T} := \{1, \ldots, T\}$, the goal of the MILP HEMS optimization problem is to minimize the following multi objective function:

$$\min_{\mathbf{P}^{\text{net}}, \boldsymbol{\delta}} J = \underbrace{\sum_{u \in \mathcal{U}} \sum_{t \in \mathcal{T}} \pi_t P^{\text{net}}_{u,t}}_{J_1} + \underbrace{\sum_{u \in \mathcal{U}} \epsilon_u \sum_{t \in \mathcal{T}} \delta_{u,t}}_{J_2}. \quad (1)$$

J_1 is the daily electricity cost of consumers in terms of the electricity price π_t and the net consumption $P^{\text{net}}_{u,t}$.

TABLE 1. Notation.

$\widehat{P}^{\text{solar}}_{u,t}$	Solar generation in consumer u, phase p at time t
$P^{\text{net}}_{u,t}$	Net power consumption in consumer u at time t
$P_{p,u,a,t}$	Power consumption of the appliance a for consumer u, phase p at time t
$P^{\text{max(min)}}_{p,u,a}$	Maximum(Minimum) power consumption of the appliance a in consumer u, phase p
$P^{\text{c(d)}}_{p,u,a,t}$	Charging(Discharging) power of the ESS a in consumer u, phase p at time t
$P^{\text{c,max(min)}}_{p,u,a}$	Maximum(Minimum) charging power of the ESS a in consumer u, phase p
$P^{\text{d,max(min)}}_{p,u,a}$	Maximum(Minimum) discharging power of the ESS a in consumer u, phase p
$SOC_{p,u,a,t}$	State of the charge of the ESS a in consumer u, phase p at time t
$SOC^{\text{max(min)}}_{p,u,a}$	Maximum(Minimum) charge state of the ESS a in consumer u, phase p
$\eta^{\text{c(d)}}_{p,u,a}$	Charging(Discharging) efficiency of the ESS a in consumer u, phase p
$E^{\text{max(min)}}_{p,u,a}$	Maximum(Minimum) energy capacity of the ESS a in consumer u, phase p
$b_{p,u,a,t}$	Charging state of the ESS a in consumer u, phase p at time t; "1" for charging and "0" otherwise
$y_{p,u,a,t}$	Consumption state of a non-interruptible shiftable appliance a in consumer u, phase p at time t; "1" for consumption and "0" otherwise
$\alpha_{p,u}, \beta_{p,u}$	Thermal characteristics for air conditioner in consumer u, phase p
$d_{p,u,a}$	Operation period (hours) during a day for non-interruptible load a in consumer u, phase p
$a_{p,u,l}$	Element of a node-branch matrix in consumer u, phase p
$F^{\text{max}}_{p,l}$	Maximum flow limits for the distribution line l, phase p
π_t	Electricity price at time t
$\delta_{p,u,t}$	Deviation of preferred indoor temperature in consumer u, phase p at time t
$\epsilon_{p,u}$	Penalty for the relaxation variable in consumer u, phase p
$\delta^{\text{max}}_{p,u}$	Maximum deviation of preferred temperature in consumer u, phase p
$T^{\text{in}}_{p,u,a,t}$	The indoor temperature by the appliance a in consumer u, phase p at time t
$T^{\text{max(min)}}_{p,u}$	Maximum(Minimum) comfortable temperature in consumer u, phase p
$Q_{p,u}$	Demand reduction request in consumer u, phase p
$D_{p,u}$	Demand response period in consumer u, phase p
$V_{i,p}(V^z_{i,p})$	Voltage magnitude (measurement) at bus i for phase p
$\theta_{i,p}$	Voltage angle at bus i for phase p
$P_{i,p}(P^z_{i,p})$	Real power injection (measurement) at bus i, phase p
$Q_{i,p}(Q^z_{i,p})$	Reactive power injection (measurement) at bus i, phase p
$P_{ij,p}(P^z_{ij,p})$	Real power flow (measurement) from bus i to bus j for phase p
$Q_{ij,p}(Q^z_{ij,p})$	Reactive power flow (measurement) from bus i to bus j for phase p
$I_{ij,p}(I^z_{ij,p})$	Current magnitude (measurement) from bus i to bus j for phase p
$\omega^V_{i,p}$	Weight for voltage measurement at bus i for phase p
$\omega^{P(Q)}_{i,p}$	Weight for real (reactive) power injection measurement at bus i for phase p
$\omega^{P(Q)}_{ij,p}$	Weight for real (reactive) power flow measurement from bus i to bus j for phase p
$\omega^I_{ij,p}$	Weight for current measurement from bus i to bus j, phase p
$P^{\text{max(min)}}_{i,p}$	Maximum(Minimum) real power generation at bus i, phase p
$Q^{\text{max(min)}}_{i,p}$	Maximum(Minimum) reactive power generation at bus i, phase p
$\theta^{\text{max(min)}}_{i,p}$	Maximum(Minimum) voltage angle at bus i, phase p
$G(B)_{ij,pq}$	Real (Imaginary) part of ijth element of the complex bus admittance matrix, phase p to q
$g(b)_{ij,pq}$	Real (Imaginary) part of the admittance of the series branch connecting buses i and j, phase p to q

J_2 is the amount of the consumer' discomfort cost that includes the deviation of the consumer' preferred temperature from the indoor temperature. The relaxation variable $\delta_{u,t}$ is

the temperature deviation of the consumer u, and the feasibility of the optimization problem can be guaranteed by $\delta_{u,t}$ with the penalty parameter ϵ_u at the expense of the consumer preferred thermal comfort. With the objective function, the HEMS optimization problem is formulated with the following equality/inequality constraints:

$$P^{\text{net}}_{u,t} = \sum_{a\in\mathcal{A}^{c}_{u,r}} P_{u,a,t} + \sum_{a\in\mathcal{A}^{c,NI}_{u,s}} P_{u,a,t} + \sum_{a\in\mathcal{A}^{c,I}_{u,s}} \left(P^{\text{c}}_{u,a,t} - P^{\text{d}}_{u,a,t}\right) + \sum_{a\in\mathcal{A}^{uc}_{u}} P_{u,a,t} - \widehat{P}^{\text{solar}}_{u,t} \tag{2}$$

$$T^{\text{in}}_{u,a,t} = T^{\text{in}}_{u,a,t-1} + \alpha_u(\widehat{T}^{\text{out}}_{u,t-1} - T^{\text{in}}_{u,a,t-1}) + \beta_u P_{u,a,t} \quad \forall a \in A^{c}_{u,r} \tag{3}$$

$$\sum_{t\in\mathcal{T}} y_{u,a,t} = d_{u,a}, \quad \forall a \in \mathcal{A}^{c,NI}_{u,s} \tag{4}$$

$$\sum_{t\in\mathcal{T}} v_{u,a,t} = 1, \quad \forall a \in \mathcal{A}^{c,NI}_{u,s} \tag{5}$$

$$y_{u,a,t} = \sum_{\tau=t-L_{u,a}+1}^{t} v_{u,a,\tau}, \quad \forall a \in \mathcal{A}^{c,NI}_{u,s} \tag{6}$$

$$SOC_{u,a,t} = SOC_{u,a,t-1} + \frac{\eta^{\text{c}}_{u,a} P^{\text{c}}_{u,a,t}}{E^{\max}_{u,a}} - \frac{P^{\text{d}}_{u,a,t}}{\eta^{\text{d}}_{u,a} E^{\max}_{u,a}} \quad \forall a \in \mathcal{A}^{c,I}_{u,s} \tag{7}$$

$$P^{\text{net}}_{u,t} = \sum_{l\in\mathcal{L}} a_{u,l} F_{l,t} \tag{8}$$

$$F_{1,t} = \sum_{u\in\mathcal{U}} P^{\text{net}}_{u,t} \tag{9}$$

$$P^{\text{net}}_{u,t} \le \text{DR}(\text{Q}_u, \text{D}_u) \tag{10}$$

$$T^{\min}_{u} - \delta_{u,t} \le T^{\text{in}}_{u,a,t} \le T^{\max}_{u} + \delta_{u,t}, \quad \forall a \in A^{c}_{u,r} \tag{11}$$

$$0 \le \delta_{u,t} \le \delta^{\max}_{u} \tag{12}$$

$$SOC^{\min}_{u} \le SOC_{u,a,t} \le SOC^{\max}_{u}, \quad \forall a \in \mathcal{A}^{c,I}_{u,s} \tag{13}$$

$$P^{\text{c,min}}_{u,a} b_{u,a,t} \le P^{\text{c}}_{u,a,t} \le P^{\text{c,max}}_{u,a} b_{u,a,t}, \quad \forall a \in \mathcal{A}^{c,I}_{u,s} \tag{14}$$

$$P^{\text{d,min}}_{u,a}(1 - b_{u,a,t}) \le P^{\text{d}}_{u,a,t} \le P^{\text{d,max}}_{u,a}(1 - b_{u,a,t}), \tag{15}$$

$$P^{\min}_{u,a} \le P_{u,a,t} \le P^{\max}_{u,a}, \quad \forall a \in \mathcal{A}^{c}_{u,r}/\mathcal{A}^{c,I}_{u,s} \tag{16}$$

$$-F^{\max}_{l} \le F_{l,t} \le F^{\max}_{l}, \quad \forall l \in \mathcal{L}. \tag{17}$$

Equation (2) is the constraint on the net energy consumption (total consumption of the reducible appliance ($a \in \mathcal{A}^{c}_{u,r}$), shiftable appliances with non-interruptible load ($a \in \mathcal{A}^{c,NI}_{u,s}$), shiftable appliances with interruptible load ($a \in \mathcal{A}^{c,I}_{u,s}$), and uncontrollable appliances ($a \in \mathcal{A}^{uc}_{u}$) without the predicted solar generation). Equation (3) is the constraint for the temperature dynamics of the reducible appliance at the hour t ($T^{\text{in}}_{u,a,t}$) in terms of $T^{\text{in}}_{u,a,t-1}$ of hour $t-1$, the outdoor temperature at hour $t-1$ ($\widehat{T}^{\text{out}}_{u,t-1}$), the reducible appliance power consumption ($P_{u,a,t}$), and the environmental parameters (α_u, β_u) that specify the indoor thermal condition. Equations eqs. (4)–(6) guarantee the desired operations of shiftable appliances with the non-interruptible load (e.g., washer): i) for the operation period $d_{u,a}$ hours during a day (4), ii) for the starting time with once-daily binary value (5); and iii) a consecutive operation period $d_{u,a}$ hours (6). Equation (7) defines the operational dynamics of the state of charge (SOC) for the ESS at the current hour t in terms of the SOC at the previous hour $t-1$, the battery capacity $E^{\max}_{u,a}$, the charging and discharging efficiency, $\eta^{c}_{u,a}$ and $\eta^{d}_{u,a}$, and the charging and discharging power, $P^{\text{c}}_{u,a,t}$ and $P^{\text{d}}_{u,a,t}$. Equation (8) illustrates the relationship between the consumer u' net power and the power flows to his neighbors. In (8), $a_{u,l}$ is the element of a node-branch matrix $\mathbf{A}$, as follows: $a_{u,l} = \pm 1$ if the node u is the receiving or sending terminal of the branch $l \in \mathcal{L}$; otherwise $a_{u,l} = 0$. Equation (9) is the total power flow from a grid, which is equal to the sum of the net consumptions of all of the consumers. The DR constraint is illustrated in (10), where the DR signal consists of the demand reduction requests Q_u KW and the DR period of D_u hours. Equation (11) presents the range of the relaxed indoor temperature, which is limited by $\delta^{\max}_{u}$ in (12). Equation (13) is the capacity constraint of the SOC. Equations (14) and (15) are the constraints on the charging and discharging powers of the ESS, where $b_{u,a,t}$ represents the binary decision variable that determines the on/off status of the ESS. The capacity of the power consumption for the shiftable appliances with the non-interruptible load and reducible appliances is described in (16). The inter-consumer power flow is limited in (17).

B. DISTRIBUTION SYSTEM STATE ESTIMATION

In an MV distribution network, a three-phase unbalanced weighted least squares (WLS) DSSE is formulated, as shown in [32],

$$\min_{\mathbf{V},\boldsymbol{\theta},\mathbf{P},\mathbf{Q},\mathbf{P}_F,\mathbf{Q}_F,\mathbf{I}} J = \sum_{p=a,b,c}\Bigg[\sum_{i\in\mathcal{B}_V}\omega^{V}_{i,p}(V^{z}_{i,p} - V_{i,p})^2 + \sum_{i\in\mathcal{B}_{P_I}}\omega^{P}_{i,p}(P^{z}_{i,p} - P_{i,p})^2 + \sum_{i\in\mathcal{B}_{Q_I}}\omega^{Q}_{i,p}(Q^{z}_{i,p} - Q_{i,p})^2 + \sum_{(i,j)\in\mathcal{B}_{P_F}}\omega^{P}_{ij,p}(P^{z}_{ij,p} - P_{ij,p})^2 + \sum_{(i,j)\in\mathcal{B}_{Q_F}}\omega^{Q}_{ij,p}(Q^{z}_{ij,p} - Q_{ij,p})^2 + \sum_{(i,j)\in\mathcal{B}_I}\omega^{I}_{ij,p}(I^{z}_{ij,p} - I_{ij,p})^2\Bigg] \tag{18}$$

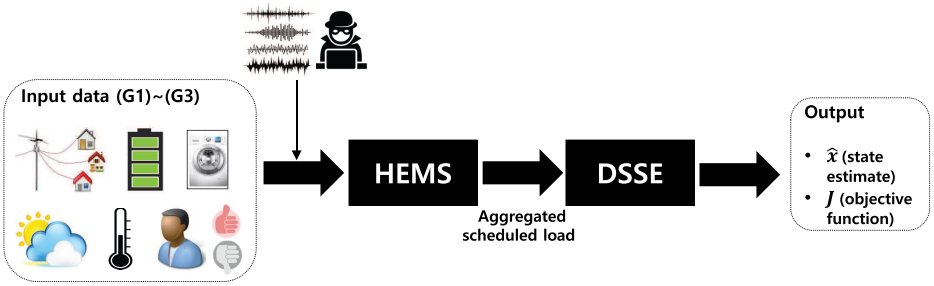

FIGURE 2. Impact of the data change in the HEMS on the DSSE.

s.t.

$$P_{i,p} = V_{i,p} \sum_{j\in\mathcal{N}_i} \sum_{q=a,b,c} \Big[V_{j,q}\{G_{ij,pq}\cos(\theta_{i,p}-\theta_{j,q}) + B_{ij,pq}\sin(\theta_{i,p}-\theta_{j,q})\}\Big] \tag{19}$$

$$Q_{i,p} = V_{i,p} \sum_{j\in\mathcal{N}_i} \sum_{q=a,b,c} \Big[V_{j,q}\{G_{ij,pq}\sin(\theta_{i,p}-\theta_{j,q}) - B_{ij,pq}\cos(\theta_{i,p}-\theta_{j,q})\}\Big] \tag{20}$$

$$\begin{aligned} P_{ij,p} = V_{i,p} \sum_{q=a,b,c} \Big[& V_{i,q}\{g_{ij,pq}\cos(\theta_{i,p}-\theta_{i,q}) \\ & + b_{ij,pq}\sin(\theta_{i,p}-\theta_{i,q})\} \\ & + V_{j,q}\{-g_{ij,pq}\cos(\theta_{i,p}-\theta_{j,q}) \\ & - b_{ij,pq}\sin(\theta_{i,p}-\theta_{j,q})\}\Big] \end{aligned} \tag{21}$$

$$\begin{aligned} Q_{ij,p} = V_{i,p} \sum_{q=a,b,c} \Big[& V_{i,q}\{g_{ij,pq}\sin(\theta_{i,p}-\theta_{i,q}) \\ & - b_{ij,pq}\cos(\theta_{i,p}-\theta_{i,q})\} \\ & + V_{j,q}\{-g_{ij,pq}\sin(\theta_{i,p}-\theta_{j,q}) \\ & + b_{ij,pq}\cos(\theta_{i,p}-\theta_{j,q})\}\Big] \end{aligned} \tag{22}$$

$$I_{ij,p} = \sum_{q=a,b,c} \Big[(g_{ij,pq}^2 + b_{ij,pq}^2)\{V_{i,q}^2 + V_{j,q}^2 - 2V_{i,q}V_{j,q}\cos(\theta_{i,q}-\theta_{j,q})\}\Big]^{\frac{1}{2}} \tag{23}$$

$$P_{i,p}^{\min}(Q_{i,p}^{\min}) \le P_{i,p}(Q_{i,p}) \le P_{i,p}^{\max}(Q_{i,p}^{\max}) \tag{24}$$

$$\theta_{i,p}^{\min} \le \theta_{i,p} \le \theta_{i,p}^{\max}. \tag{25}$$

The goal of the previous optimization problem is the computation of the optimal estimate of the state variable vector $\mathbf{V}$ and $\boldsymbol{\theta}$ (the estimates of $\mathbf{P}, \mathbf{Q}, \mathbf{P}_F, \mathbf{Q}_F$, and $\mathbf{I}$ are determined from the estimates of $\mathbf{V}$ and $\boldsymbol{\theta}$) through the minimization of the weighted measurement error function J in (18) while the equality/inequality constraints are being satisfied eqs. (19)–(25). In (18), the sets $\left(\mathcal{B}_V, \mathcal{B}_{P_I}, \mathcal{B}_{Q_I}, \mathcal{B}_{P_F}, \mathcal{B}_{Q_F}, \text{and } \mathcal{B}_I\right)$ include buses with voltage magnitude measurements, real/reactive power injection measurements, real/reactive power flow measurements, and current magnitude measurements, respectively. Equations (19) and (20) are the real and reactive power injection constraints, respectively. Equations (21) and (22) are the real and reactive power flow constraints, respectively. The current magnitude constraint is illustrated in (23). The inequality constraints eqs. (24) and (25) enforce the limits of real power generations, reactive power generations, and voltage angles, respectively.

III. PROPOSED SENSITIVITY ANALYSIS FRAMEWORK

This section introduces the proposed analysis framework that is used to quantify the DSSE sensitivity with respect to data changes in the HEMS. In the proposed framework, we consider the situation where the HEMS data changes due to a natural noise and/or a data attack could distort the HEMS solution (i.e., aggregate scheduled load), which in turn leads to incorrect DSSE solutions such as the estimated states and the objective function as shown in Fig. 2,.

A. SENSITIVITY ANALYSIS IN AN OPTIMIZATION PROBLEM

A general nonlinear programming optimization problem is formulated as follows:

$$\min_{\mathbf{x}} J(\mathbf{x}, \mathbf{a}) \tag{26}$$

$$\text{s.t. } \boldsymbol{\lambda} : \mathbf{f}(\mathbf{x}, \mathbf{a}) = \mathbf{0}, \quad \boldsymbol{\kappa} : \mathbf{g}(\mathbf{x}, \mathbf{a}) \le \mathbf{0}, \tag{27}$$

where $J(\mathbf{x}, \mathbf{a})$ is a scalar objective function, and $\mathbf{f}(\mathbf{x}, \mathbf{a})$ and $\mathbf{g}(\mathbf{x}, \mathbf{a})$ are the equality and inequality constraints with the corresponding Lagrangian multipliers $\boldsymbol{\lambda}$ and $\boldsymbol{\kappa}$, respectively. $\mathbf{x}$ is the decision variable vector and $\mathbf{a}$ is the data vector that is used for the formulation of the optimization problem.

1) KKT CONDITIONS

Given the Lagrangian function ($\mathcal{L}(\mathbf{x}, \mathbf{a}) = J(\mathbf{x}, \mathbf{a}) + \boldsymbol{\lambda}\mathbf{f}(\mathbf{x}, \mathbf{a}) + \boldsymbol{\kappa}\mathbf{g}(\mathbf{x}, \mathbf{a})$), the KKT conditions are written as follows:

(K1) $\nabla_{\mathbf{x}}\mathcal{L}(\mathbf{x}, \mathbf{a}) = \mathbf{0} \Rightarrow \nabla_{\mathbf{x}} J(\mathbf{x}, \mathbf{a}) + \boldsymbol{\lambda}\nabla_{\mathbf{x}}\mathbf{f}(\mathbf{x}, \mathbf{a}) + \boldsymbol{\kappa}\nabla_{\mathbf{x}}\mathbf{g}(\mathbf{x}, \mathbf{a}) = \mathbf{0}$,
(K2) $\mathbf{f}(\mathbf{x}, \mathbf{a}) = \mathbf{0}$,
(K3) $\mathbf{g}(\mathbf{x}, \mathbf{a}) \le \mathbf{0}$,
(K4) $\boldsymbol{\kappa}\mathbf{g}(\mathbf{x}, \mathbf{a}) = \mathbf{0}, \boldsymbol{\kappa} \ge \mathbf{0}$,

where (K2) and (K3) are the primal feasibility conditions, and (K4) is either the dual feasibility or the complimentary slackness conditions. In this paper, only the binding inequality constraints ($\boldsymbol{\kappa} > \mathbf{0}$) are considered for our sensitivity analysis.

2) PERTURBED KKT CONDITIONS

The perturbed equations of the previously mentioned KKT conditions that are subject to $\mathbf{x}$, $\mathbf{a}$, $\boldsymbol{\lambda}$, and $\boldsymbol{\kappa}$, are written as follows:

(P1) $[\nabla_{\mathbf{x}} J(\mathbf{x}, \mathbf{a})]^T d\mathbf{x} + [\nabla_{\mathbf{a}} J(\mathbf{x}, \mathbf{a})]^T d\mathbf{a}\text{-}dJ = 0$

(P2) $[\nabla_{\mathbf{xx}} J(\mathbf{x}, \mathbf{a}) + \boldsymbol{\lambda} \nabla_{\mathbf{xx}} \mathbf{f}(\mathbf{x}, \mathbf{a}) + \boldsymbol{\kappa} \nabla_{\mathbf{xx}} \mathbf{g}(\mathbf{x}, \mathbf{a})] d\mathbf{x}$
$+ [\nabla_{\mathbf{xa}} J(\mathbf{x}, \mathbf{a}) + \boldsymbol{\lambda} \nabla_{\mathbf{xa}} \mathbf{f}(\mathbf{x}, \mathbf{a}) + \boldsymbol{\kappa} \nabla_{\mathbf{xa}} \mathbf{g}(\mathbf{x}, \mathbf{a})] d\mathbf{a}$
$+ \nabla_{\mathbf{x}} (\mathbf{f}(\mathbf{x}, \mathbf{a})) d\boldsymbol{\lambda} + \nabla_{\mathbf{x}} (\mathbf{g}(\mathbf{x}, \mathbf{a})) d\boldsymbol{\kappa} = \mathbf{0}$,

(P3) $[\nabla_{\mathbf{x}} \mathbf{f}(\mathbf{x}, \mathbf{a})]^T d\mathbf{x} + [\nabla_{\mathbf{a}} \mathbf{f}(\mathbf{x}, \mathbf{a})]^T d\mathbf{a} = \mathbf{0}$,

(P4) $[\nabla_{\mathbf{x}} \mathbf{g}(\mathbf{x}, \mathbf{a})]^T d\mathbf{x} + [\nabla_{\mathbf{a}} \mathbf{g}(\mathbf{x}, \mathbf{a})]^T d\mathbf{a} = \mathbf{0}$.

Using (P1)∼(P4), the following linear matrix equation is constructed,

$$\mathbf{S_1} [d\mathbf{x}\ d\boldsymbol{\lambda}\ d\boldsymbol{\kappa}\ dJ]^T = \mathbf{S_2} d\mathbf{a} \tag{28}$$

where $\mathbf{S_1}$ and $\mathbf{S_2}$ are the matrices whose elements are the coefficients of $d\mathbf{x}$, $d\mathbf{a}$, $d\boldsymbol{\lambda}$, $d\boldsymbol{\kappa}$, and dJ in the perturbed KKT conditions (detailed expressions of $\mathbf{S_1}$ and $\mathbf{S_2}$ are referred in [26]).

Lastly, the matrix $\mathbf{S} = \mathbf{S_1^{-1}} \mathbf{S_2}$ provides the sensitivity of the decision variables, the Lagrangian multipliers, and the objective function with respect to the data variations.

$$\mathbf{S} = \mathbf{S_1^{-1}} \mathbf{S_2} = \left[\frac{d\mathbf{x}}{d\mathbf{a}} \frac{d\boldsymbol{\lambda}}{d\mathbf{a}} \frac{d\boldsymbol{\kappa}}{d\mathbf{a}} \frac{dJ}{d\mathbf{a}} \right]^T. \tag{29}$$

Remark 1: The previously mentioned sensitivity analysis approach can be applied to the MILP optimization problem for the HEMS in the following steps:

Step 1) The solution of the MILP problem is calculated

Step 2) The MILP problem is converted into the LP problem through a consideration of the obtained integer decision variables from Step 1) as the fixed data, the constraints that include only the integer decision variables are eliminated, and the solution of this modified LP problem is calculated.

Step 3) For the binding constraints, the redundant constraints and the nonbasic variables are removed to ensure the invertibility of the matrix $\mathbf{M}_1$ in (29), the explanation of which is given in [27].

B. PROPOSED SENSITIVITY MATRIX

First, using the KKT conditions perturbation approach that is introduced in subsection III-A, the desired sensitivity matrices of the HEMS and the DSSE (i.e, a truncated matrix of (29) without a consideration of the Lagrangian multipliers) can be derived, respectively,

$$\mathbf{S}_{\text{HEMS}} = \frac{d\mathbf{L}}{d\mathbf{a}}, \quad \mathbf{S}^{\widehat{\mathbf{x}}}_{\text{DSSE}} = \frac{d\widehat{\mathbf{x}}}{d\mathbf{b}}, \quad \mathbf{S}^{J}_{\text{DSSE}} = \frac{dJ}{d\mathbf{b}}, \tag{30}$$

where $\mathbf{L}$ is the vector function in terms of the aggregate scheduled load $L_i[t] = \sum_{u \in \mathcal{U}} P^{\text{net}}_{u,t}$ at the time slot t for load bus i, and the data vectors of the HEMS and the DSSE from eqs. (1)–(17) and eqs. (18)–(25) are written as

$$\mathbf{a} = [\boldsymbol{\alpha}\ \boldsymbol{\eta}^{\text{c(d)}}\ \mathbf{SOC}^{\text{cap}}\ \mathbf{T}^{\text{cap}}\ \boldsymbol{\delta}^{\max}\ \mathbf{P}^{\text{c(d),cap}}\ \mathbf{F}^{\max}\ \mathbf{DR}\ \mathbf{P}^{\text{solar}}]^T,$$
$$\mathbf{b} = [\mathbf{V}^z\ \mathbf{P}^z_I\ \mathbf{Q}^z_I\ \mathbf{P}^z_F\ \mathbf{Q}^z_F\ \mathbf{I}^z].$$

In the vector $\mathbf{a}$, a superscript cap represents the maximum or minimum value of the variable.

The following two subsections provide simple numerical examples how to derive the KKT and the perturbed KKT conditions for HEMS and DSSE. For simplicity, we consider equality/inequality constraints (9), (10) for HEMS and equality constraint (19) for DSSE.

1) HEMS SENSITIVITY ANALYSIS FRAMEWORK

The Lagrangian function of the simplified HEMS optimization problem is formulated as

$$\begin{aligned}\mathcal{L} = &\sum_{u \in \mathcal{U}} \sum_{t \in \mathcal{T}} \pi_t P^{\text{net}}_{u,t} + \sum_{u \in \mathcal{U}} \epsilon_u \sum_{t \in \mathcal{T}} \delta_{u,t} \\ &- \sum_{t \in \mathcal{T}} \lambda_t \left(F_{1,t} - \sum_{u \in \mathcal{U}} P^{\text{net}}_{u,t} \right) \\ &+ \sum_{u \in \mathcal{U}} \sum_{t \in \mathcal{T}} \kappa_{u,t} \left(P^{\text{net}}_{u,t} - \text{DR}(\text{Q}_u, \text{D}_u) \right).\end{aligned} \tag{31}$$

Then, the KKT first-order conditions for the HEMS model are expressed as

(C1) $(\pi_t + \lambda_t + \kappa_{u,t}) \chi_{\{(u,t) \in \mathcal{U} \times \mathcal{T}\}} = 0, \quad \forall u, t$

(C2) $\epsilon_u \chi_{\{(u,t) \in \mathcal{U} \times \mathcal{T}\}} = 0, \quad \forall u, t$

(C3) $\lambda_t \chi_{\{t \in \mathcal{T}\}} = 0, \quad \forall t$

(C4) $F_{1,t} = \sum_{u \in \mathcal{U}} P^{\text{net}}_{u,t}, \quad \forall t$

(C5) $P^{\text{net}}_{u,t} = \text{DR}(\text{Q}_u, \text{D}_u), \quad \forall u, t.$

Here, $\chi_{\{(u,t) \in A\}}$ and $\chi_{\{t \in A\}}$ are the characteristic functions based on the set A. Next, all KKT equations (C1)∼(C5) along with the HEMS objective function are perturbed in regards to the decision variables ($P^{\text{net}}_{u,t}$, $\delta_{u,t}$, and $F_{1,t}$), Lagrange multipliers ($\lambda_{u,t}$ and $\kappa_{u,t}$), and data (π_t, ϵ_u, and $\text{DR}(\text{Q}_u, \text{D}_u)$) as long as the KKT conditions still hold. All perturbed equations for the HEMS are finally written in a linear matrix equation form as follows:

$$\begin{bmatrix} \mathbf{M}_1 & \mathbf{0} & -1 & 0 \\ \mathbf{M}_2 & \mathbf{0} & 0 & -1 \\ \mathbf{0} & \boldsymbol{\Upsilon}^T & 0 & 0 \\ \boldsymbol{\Upsilon} & \mathbf{0} & 0 & 0 \end{bmatrix} \begin{bmatrix} d\mathbf{P}^{\text{net}} \\ d\boldsymbol{\delta} \\ dF_1 \\ d\boldsymbol{\lambda} \\ d\boldsymbol{\kappa} \\ dJ_1 \\ dJ_2 \end{bmatrix} = \begin{bmatrix} \boldsymbol{\Lambda}_1 \\ \boldsymbol{\Lambda}_2 \\ \boldsymbol{\Lambda}_3 \end{bmatrix} \begin{bmatrix} d\boldsymbol{\pi} \\ d\boldsymbol{\epsilon} \\ d\mathbf{DR} \end{bmatrix}. \tag{32}$$

Taking the inverse of the left-hand side matrix in (32) on both sides of (32), we can obtain the sensitivity matrix that evaluates the impact of HEMS data on aggregate scheduled load. The derivations of submatrices in the linear matrix equation (32) are referred to in Appendix A.

2) DSSE SENSITIVITY ANALYSIS FRAMEWORK

The Lagrangian function of the simplified DSSE optimization problem is formulated as

$$\mathcal{L} = \sum_{p=a,b,c} \Bigg[\sum_{i \in \mathcal{B}_{P_I}} \omega^P_{i,p} (P^z_{i,p} - P_{i,p})^2 - \sum_{i \in \mathcal{B}_{P_I}} \lambda_{i,p} \Bigg(P_{i,p} - V_{i,p} \sum_{j \in \mathcal{N}_i} \sum_{q=a,b,c} \Big[V_{j,q} \{ G_{ij,pq} \cos(\theta_{i,p} - \theta_{j,q}) + B_{ij,pq} \sin(\theta_{i,p} - \theta_{j,q}) \} \Big] \Bigg) \Bigg]. \tag{33}$$

Then, the KKT first-order conditions for the DSSE model are expressed as

$$\begin{aligned}
&\text{(D1)} \Bigg(\sum_{j \in \mathcal{N}_i} \sum_{q=a,b,c} \lambda_{i,p} \Big[V_{j,q} \{ G_{ij,pq} \cos(\theta_{i,p} - \theta_{j,q}) + B_{ij,pq} \sin(\theta_{i,p} - \theta_{j,q}) \} \Big] + V_{i,p} G_{ii,pp} \Bigg) \\
&\quad + \sum_{o=a,b,c, o \neq p} \lambda_{i,o} \Big[V_{j,p} \{ G_{ij,po} \cos(\theta_{i,p} - \theta_{i,o}) + B_{ii,po} \sin(\theta_{i,p} - \theta_{i,o}) \} \Big] + \sum_{j \in \mathcal{N}_B, j \neq i} \sum_{q=a,b,c} \lambda_{j,p} \\
&\quad \Big[V_{i,p} \{ G_{ij,pq} \cos(\theta_{i,p} - \theta_{j,q}) + B_{ij,pq} \sin(\theta_{i,p} - \theta_{j,q}) \} \Big] = 0 \\
&\text{(D2)} \Bigg(V_{i,p} \sum_{j \in \mathcal{N}_i} \sum_{q=a,b,c} \lambda_{i,p} \Big[V_{j,q} \{ -G_{ij,pq} \sin(\theta_{i,p} - \theta_{j,q}) + B_{ij,pq} \cos(\theta_{i,p} - \theta_{j,q}) \} \Big] - V^2_{i,p} B_{ii,pp} \Bigg) \\
&\quad + \sum_{o=a,b,c, o \neq p} \lambda_{i,o} \Big[V_{j,p} \{ G_{ij,po} \cos(\theta_{i,p} - \theta_{i,o}) + B_{ii,po} \sin(\theta_{i,p} - \theta_{i,o}) \} \Big] + \sum_{j \in \mathcal{N}_B, j \neq i} \sum_{q=a,b,c} \lambda_{j,p} \\
&\quad \Big[V_{i,p} \{ G_{ij,pq} \cos(\theta_{i,p} - \theta_{j,q}) + B_{ij,pq} \sin(\theta_{i,p} - \theta_{j,q}) \} \Big] = 0 \\
&\text{(D3)} \ -2\omega^P_{k,p} (P^z_{k,p} - P_{k,p}) - \lambda_{i,p} = 0 \\
&\text{(D4)} \ P_{i,p} = V_{i,p} \sum_{j \in \mathcal{N}_i} \sum_{q=a,b,c} \Big[V_{j,q} \{ G_{ij,pq} \cos(\theta_{i,p} - \theta_{j,q}) + B_{ij,pq} \sin(\theta_{i,p} - \theta_{j,q}) \} \Big].
\end{aligned}$$

Here, a symbol o represents one of the phases, however it does not equal to phase p. All KKT equations (D1)∼(D4) along with the DSSE objective function are perturbed in regards to the decision variables ($V_{i,p}$, $\theta_{i,p}$, and $P_{i,p}$), Lagrange multiplier $\lambda_{u,t}$, and data $P^z_{i,p}$ as long as the KKT conditions still hold. All perturbed equations for the DSSE are finally written in a linear matrix equation form as follows:

$$\begin{bmatrix} \mathbf{M} & \mathbf{0} & -1 \\ \boldsymbol{\Upsilon}_1 & \boldsymbol{\Upsilon}_2^T & 0 \\ \boldsymbol{\Upsilon}_2 & \mathbf{0} & 0 \end{bmatrix} \begin{bmatrix} d\mathbf{V} \\ d\boldsymbol{\theta} \\ d\mathbf{P} \\ d\boldsymbol{\lambda} \\ dJ \end{bmatrix} = \begin{bmatrix} \Big[2\omega^P_{k,p} (P^z_{k,p} - P_{k,p}) \Big]_{1 \times |\mathcal{B}_{P_I}|} \\ \mathbf{0}_{|\mathcal{B}_{P_I}| \times |\mathcal{B}_{P_I}|} \\ \boldsymbol{\Lambda} \end{bmatrix} \Big[d\mathbf{P}^z_I \Big]. \tag{34}$$

Taking the inverse of the left-hand side matrix in (34) on both sides of (34), we can obtain the sensitivity matrix that assesses the impact of DSSE data (in particular, real power injection measurement) on DSSE solutions. The derivations of submatrices in the linear matrix equation (34) are referred to in Appendix B.

TABLE 2. Classification of data in HEMS.

Group	Unit	Data
(G1)	Power rating (W)	$F_l^{\max}$, DR, $P_u^{\mathrm{c,max(min)}}$, $P_u^{\mathrm{d,max(min)}}$, P_u^{solar}
(G2)	Temperature (°C)	$T_u^{\max(\min)}$, $\delta_u^{\max}$
(G3)	No unit	α_u, η_u^{c}, η_u^{d}, $SOC_u^{\max(\min)}$

In this paper, the considered HEMS data are classified into three groups ((G1) ∼ (G3)) according to the data unit in Table 2. The first group includes the capacity limits of the flow line, the ESS charge/discharge, the DR signal, and the solar power generation. The second group corresponds to the comfortable indoor temperature range and the relaxed temperature of the consumer. In the third group, the data represent the parameters of the indoor thermal condition and the ESS.

Next, the composite functions of $\widehat{\mathbf{x}}(\mathbf{L}(\mathbf{a}))$ and $J(\mathbf{L}(\mathbf{a}))$ that explain the relationship between the HEMS data $\mathbf{a}$ and the DSSE solution including the state estimate $\widehat{\mathbf{x}}$ and the objective function J, respectively, are defined. To develop the desired sensitivity framework, the following assumptions are considered for the two previously mentioned composite functions:

i) The HEMS scheduling time (every hour) is synchronized with the DSSE execution time (every several minutes).
ii) The aggregated load of the HEMS at any bus equals the real power injection measurement for the DSSE at the same bus (i.e., $\mathbf{L} = \mathbf{P}^z_I$).

According to the chain rule, together with these assumptions, the following sensitivity matrices are finally derived in a multiplication form, as follows:

$$\mathbf{S}^{\widehat{\mathbf{x}}} = \frac{d\widehat{\mathbf{x}}}{d\mathbf{a}} = \frac{d\widehat{\mathbf{x}}}{d\mathbf{L}} \frac{d\mathbf{L}}{d\mathbf{a}} = \mathbf{S}^{\widehat{\mathbf{x}}}_{\mathrm{DSSE}} \mathbf{S}_{\mathrm{HEMS}}, \tag{35}$$

$$\mathbf{S}^{J} = \frac{dJ}{d\mathbf{a}} = \frac{dJ}{d\mathbf{L}} \frac{d\mathbf{L}}{d\mathbf{a}} = \mathbf{S}^{J}_{\mathrm{DSSE}} \mathbf{S}_{\mathrm{HEMS}}, \tag{36}$$

where $\mathbf{L}$ is selected as the intermediate vector for which two of the different sensitivity matrices of the HEMS ($\mathbf{S}_{\mathrm{HEMS}}$) and the DSSE ($\mathbf{S}^{\widehat{\mathbf{x}}}_{\mathrm{DSSE}}$ or $\mathbf{S}^{J}_{\mathrm{DSSE}}$) are combined. The main goal of this paper is to calculate the sensitivity of the DSSE to the data changes of the HEMS using the matrices in (35) and (36).

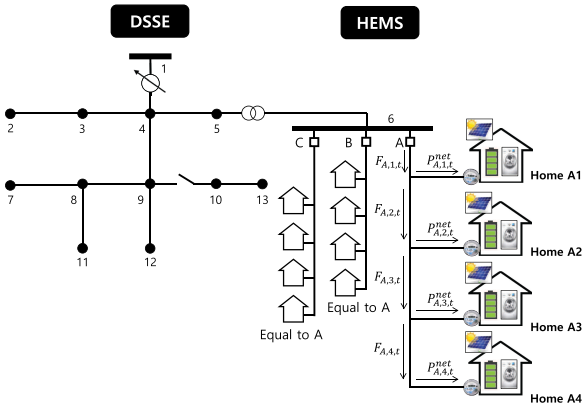

FIGURE 3. IEEE 13-bus system with 12 smart households.

IV. SIMULATION RESULTS

In this section, the sensitivity of the DSSE with respect to the HEMS data changes is illustrated in the the IEEE 13-bus MV test system [33] with 12 smart households in the LV network, as shown in Fig. 3. The smart households belong to three groups, each of which has four households that are connected to the feeder associated with bus 6 for phases A, B, and C, respectively.

For the HEMS data in four households for phase A, the total scheduling period is one day with $T = 24$ time slots so that each time slot is 1 h. It is assumed that each consumer joins a DR program and accepts a DR reduction request ($Q_{A,u} = 650$W, $D_{A,u} = 4$ h (1 P.M.∼4 P.M.)). The TOU rates are selected as follows: 0.14 \$/KWh for the peak ($10-11$ A.M., $1-4$ P.M.), 0.11 \$/KWh for the shoulder (9 A.M., 12 P.M., $5-10$ P.M.) and 0.06 \$/KWh for the off-peak period ($12-8$ A.M.). For simplicity, each consumer u has the appliances and the ESS with identical specifications, as follows: for the air conditioner $P^{\max}_{A,u,a} = 1$KW, for the washer $P^{\max}_{A,u,a} = 0.2$KW, and for ESS $\eta^{\mathrm{c}}_{A,u,a} = 0.95$, $\eta^{\mathrm{d}}_{A,u,a} = 0.9$, $E^{\max}_{A,u,a} = 400$Wh, $SOC^{\max}_{A,u} = 0.9$, $SOC^{\min}_{A,u} = 0.1$, $SOC_{A,u,0} = 0.5$, $P^{\mathrm{c,max}}_{A,u,a} = 120$W, $P^{\mathrm{c,min}}_{A,u,a} = 13$W, $P^{\mathrm{d,max}}_{A,u,a} = 135$W, $P^{\mathrm{d,min}}_{A,u,a} = 12$W. The initial indoor temperatures of the four consumers are also the same as $T^{\mathrm{in}}_0 = 26°$C, the temperature relaxation $\delta^{\max} = 1°$C, and the environmental parameters ($\alpha = 0.3$, $\beta = -0.015$). However, the comfortable temperature ranges of the consumers $u = 1, 2, 3, 4$ are set differently to: [22°C, 23°C], [22°C, 24°C], [22°C, 25°C], and [22°C, 26°C], respectively. The line flow limit $F^{\max}_{A,l}$ is set as 3.2KW. In the following subsections, three cases that correspond to the HEMS-data groups (G1), (G2), and (G3) are simulated in Table 2, respectively. In this simulation, consumers 1, 2, and 3 have binding DR constraints at different time slots: $P^{\mathrm{net}}_{A,1,t}$, $P^{\mathrm{net}}_{A,2,t}$, and $P^{\mathrm{net}}_{A,3,t}$ bind at $\mathrm{DR}_{A,1}$, $\mathrm{DR}_{A,2}$, and $\mathrm{DR}_{A,3}$ in $t \in$ [1 P.M., 4 P.M.], $t \in$ [2 P.M., 4 P.M.], $t =$ 2 P.M., respectively. A DR binding constraint does not exist for consumer 4. The aggregate scheduled load $L_{6,A}$ binds at $F^{\max}_{A,1}$ in $t =$ 12 P.M. and $t \in$ [5 P.M., 7 P.M.] We assume that the HEMS data of the other four households for each phase B and C are the same as those of the four households for phase A. System data for the IEEE 13-bus distribution test feeder are taken from MATPOWER 4.0 IEEE 13-bus distribution test case file. We assume that the measurements for voltage magnitude, real/reactive power injection, real/reactive power flow and current magnitude are corrupted by additive Gaussian noises with different variances $\sigma^2 = 10^{-6}, 2\times10^{-6}, 3\times10^{-6}$ and 4×10^{-6}, respectively. For bad data detection, the threshold of the Chi-square test follows a 95% confidence level. Numerical testing is performed with the optimization toolbox in MATLAB R2015b (IntelCore i5 CPU clocking at 3.0 GHz, with 4 GB of RAM).

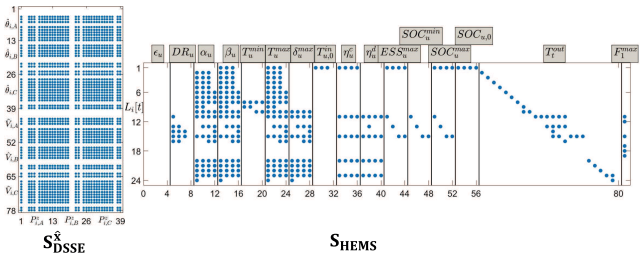

FIGURE 4. Scatter plot for the matrices $\mathbf{S}^{\hat{\mathbf{x}}}_{\mathrm{DSSE}}$ and $\mathbf{S}_{\mathrm{HEMS}}$.

A. STRUCTURE OF THE DEVELOPED SENSITIVITY MATRIX

The structure for the two developed sensitivity matrices ($\mathbf{S}^{\hat{\mathbf{x}}}_{\mathrm{DSSE}}$ and $\mathbf{S}_{\mathrm{HEMS}}$ in (35)) is illustrated in Fig. 4. The desired matrix $\mathbf{S}^{\hat{\mathbf{x}}} = \mathbf{S}^{\hat{\mathbf{x}}}_{\mathrm{DSSE}}\mathbf{S}_{\mathrm{HEMS}}$ provides the sensitivity of the DSSE three phase solutions $\hat{\mathbf{x}}$ at bus i to the HEMS data for four consumers that are connected to bus i for some phase p at time t. $d\hat{\mathbf{x}}/dL_i[t]$ and $dL_i[t]/d\mathbf{a}$ in (35) correspond to the column of $\mathbf{S}^{\hat{\mathbf{x}}}_{\mathrm{DSSE}}$ and the row of $\mathbf{S}_{\mathrm{HEMS}}$ for bus i at time t, respectively. In each sensitivity matrix, solid dots with blue color represent the elements with non-zero sensitivities. The elements with zero sensitivity are expressed without the dots. For the matrix $\mathbf{S}^{\hat{\mathbf{x}}}_{\mathrm{DSSE}}$, the x-axis indicates all real power injection measurements at any bus i for any phase p, and the y-axis indicates all voltage angle and magnitude estimates at any bus i for any phase p. For the matrix $\mathbf{S}_{\mathrm{HEMS}}$, the x-axis indicates various types of the HEMS data in the vector $\mathbf{a}$. Since all HEMS data associated with three phases are the same, the subscript p for phase is omitted. In the x-axis, $1 \sim 56$ correspond to different HEMS data for four consumers. $57 \sim 80$ and 81 represent identical data for four consumers, corresponding to $\hat{T}^{\mathrm{out}}_t$ and line flow limit, respectively. The y-axis indicates aggregate scheduled load for bus i at time t.

B. SENSITIVITY ANALYSIS FOR CHANGE IN THE HEMS DATA WITH DIFFERENT MEASUREMENT REDUNDANCY

In this subsection, we quantify the sensitivity of DSSE to changes in HEMS data under different measurement redundancy for DSSE. Figs. 5(a) and (b) show the sensitivity

TABLE 3. Sensitivities of the bus voltage angle and magnitude estimates at bus 6 for phase *C* to the change in (G1) HEMS data for a consumer.

HEMS (G1) Data	$\partial\widehat{\theta}_{6,C}/\partial a$ ($\times 10^{-3}$)	$\partial\widehat{V}_{6,C}/\partial a$ ($\times 10^{-3}$)	HEMS (G1) Data	$\partial\widehat{\theta}_{6,C}/\partial a$ ($\times 10^{-3}$)	$\partial\widehat{V}_{6,C}/\partial a$ ($\times 10^{-3}$)
$\mathrm{DR}_{C,1}$	33.64	11.18	$\widehat{P}^{\mathrm{solar}}_{C,1,11}$	3.73	1.24
$P^{c,\min}_{C,1}$	-1.37	-0.45	$\widehat{P}^{\mathrm{solar}}_{C,1,12}$	3.19	1.06
$P^{c,\max}_{C,1}$	0	0	$\widehat{P}^{\mathrm{solar}}_{C,1,13}$	4.56	1.51
$P^{d,\min}_{C,1}$	-7.46	-2.48	$\widehat{P}^{\mathrm{solar}}_{C,1,14}$	6.51	2.16
$P^{d,\max}_{C,1}$	9.56	3.18	$\widehat{P}^{\mathrm{solar}}_{C,1,15}$	9.30	3.09
$F^{\max}_{C,1}$	3.19	1.06	$\widehat{P}^{\mathrm{solar}}_{C,1,16}$	13.28	4.42
$\widehat{P}^{\mathrm{solar}}_{C,1,1\sim10}$	0	0	$\widehat{P}^{\mathrm{solar}}_{C,1,17\sim24}$	0	0

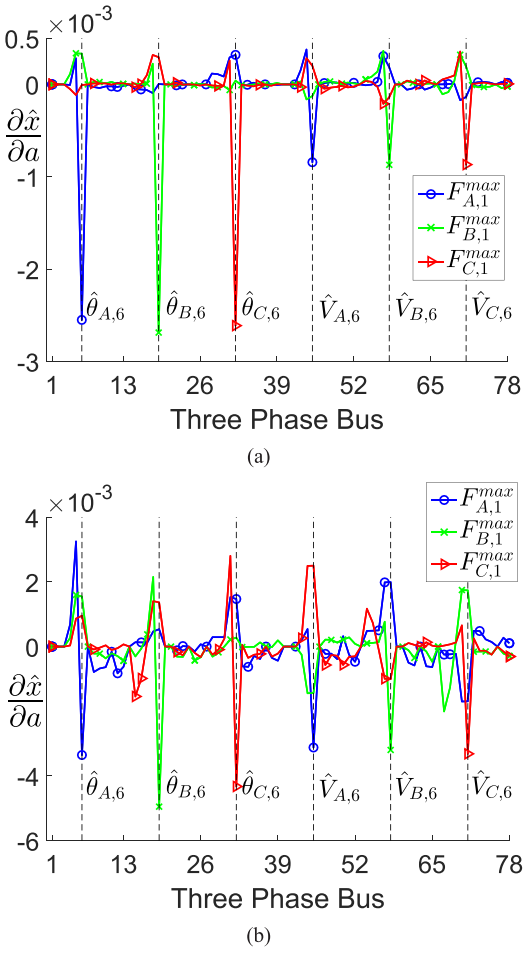

FIGURE 5. Sensitivities of the bus voltage angle and magnitude estimates at bus 6 to the change in the HEMS data under: (a) complete measurement redundancy and (b) poor measurement redundancy.

of $\widehat{V}_{i,p}$ (puV/puW) and $\widehat{\theta}_{i,p}$ (rad/puW) at any bus i for any phase p at 12 P.M. subject to line flow limit for four consumers of phases A, B, and C with complete and poor measurement redundancy, respectively. In this figure, the x-axis indices, $1 \sim 13$, $14 \sim 26$, $27 \sim 39$, $40 \sim 52$, $53 \sim 65$, and $66 \sim 78$ correspond to $\widehat{\theta}_{1\sim13,A}$, $\widehat{\theta}_{1\sim13,B}$, $\widehat{\theta}_{1\sim13,C}$, $\widehat{V}_{1\sim13,A}$, $\widehat{V}_{1\sim13,B}$, and $\widehat{V}_{1\sim13,C}$.

In Fig. 5(a), all the measurements have been completed; where the measurements of the voltage/current magnitude and the power injection/flow are assigned to each bus and line. The measurement redundancy (i.e., the ratio of the number of measurements to the number of state variables) is 225/75. We can observe from this figure that the changes of the line flow limit for each phase have little impact on voltage angle and magnitude estimates in the other phase and bus. For example, the sensitivity subject to the line flow limit for phase C has the largest absolute value in $\widehat{\theta}_{6,C}$ and $\widehat{V}_{6,C}$. This observation explains the localized effect where the intermediate variable $L_{6,C}$ at bus 6 for phase C that has been subjected to data changes is the most influential to the DSSE solution at the same bus 6 for phase C. This can be justified because the relaxed binding flow limit constraint due to increasing of $F^{\max}_{C,1}$ leads to an increase of the $L_{6,C}$, subsequently resulting in a drop of the voltage magnitude and angle estimates.

Fig. 5(b) shows the sensitivity of voltage angle and magnitude estimates under poor measurement redundancy (99/75). We can observe that the sensitivities in Fig. 5(b) are larger than the sensitivities in Fig. 5(a). This observation implies that less number of measurements causes the value of voltage magnitude and angle estimates to be more sensitive to the change of $L_{6,p}$. Moreover, compared to Fig. 5(a), the sensitivities of the voltage magnitude and angle estimates for the other buses are much larger in Fig. 5(a). We conclude from this observation that poor measurement redundancy could lead to the non-localized effect of data change on the DSSE solution.

C. SENSITIVITY ANALYSIS FOR CHANGE IN VARIOUS TYPES OF THE HEMS DATA

In this subsection, we assess the sensitivity of DSSE to changes in various types of HEMS data that are defined in Table 2. Three case studies are conducted with different data groups: (i) Case 1: (G1) data, (ii) Case 2: (G2) data; and (iii) Case 3: (G3) data, respectively. For more clear verification of the impact of the HEMS data on DSSE, the simulation setup for all three cases is the same as Fig. 5(a) with complete measurement redundancy.

1) CASE 1: SENSITIVITY ANALYSIS FOR (G1) DATA CHANGE

Table 3 shows the sensitivity of $\widehat{\theta}_{6,C}$ and $\widehat{V}_{6,C}$ at 11 A.M. subject to all data in (G1) for a consumer $C1$. From Table 3, it is verified that the (G1) data can be categorized into three sensitivity groups, each of which has the sensitivity of the

TABLE 4. Sensitivities of the estimated objective function J to the (G1) data for a consumer.

HEMS Data	$\mathrm{DR}_{C,1}$	$P^{\mathrm{c,min}}_{C,1}$	$P^{\mathrm{c,max}}_{C,1}$	$P^{\mathrm{d,min}}_{C,1}$	$P^{\mathrm{d,max}}_{C,1}$	$F^{\max}_{C,1}$	$\widehat{P}^{\mathrm{solar}}_{C,1,1\sim10}$
$\mathbf{S}^J(\times10^{-3})$	7.145	-0.29	0	-1.584	2.031	0.6774	0
HEMS Data	$\widehat{P}^{\mathrm{solar}}_{C,1,11}$	$\widehat{P}^{\mathrm{solar}}_{C,1,12}$	$\widehat{P}^{\mathrm{solar}}_{C,1,13}$	$\widehat{P}^{\mathrm{solar}}_{C,1,14}$	$\widehat{P}^{\mathrm{solar}}_{C,1,15}$	$\widehat{P}^{\mathrm{solar}}_{C,1,16}$	$\widehat{P}^{\mathrm{solar}}_{C,1,17\sim24}$
$\mathbf{S}^J(\times10^{-3})$	0.792	0.677	0.967	1.382	1.974	2.821	0

TABLE 5. Sensitivities of the bus voltage angle and magnitude estimates at bus 6 for phase C to the change in the flow limit and DR data in (G1) for 12 consumers.

(G1) HEMS Data	$\partial\widehat{\theta}_{6,C}/\partial a$ ($\times10^{-3}$)	$\partial\widehat{V}_{6,C}/\partial a$ ($\times10^{-3}$)
$\mathrm{DR}_{A,1}/\mathrm{DR}_{B,1}/\mathrm{DR}_{C,1}$	0.399 / 0.051 / **-3.263**	-0.169 / 0.241 / **-1.085**
$\mathrm{DR}_{A,2}/\mathrm{DR}_{B,2}/\mathrm{DR}_{C,2}$	0.399 / 0.051 / **-3.263**	-0.169 / 0.241 / **-1.085**
$\mathrm{DR}_{A,3}/\mathrm{DR}_{B,3}/\mathrm{DR}_{C,3}$	-0.399 / -0.051 / **3.263**	0.169 / -0.241 / **1.085**
$\mathrm{DR}_{A,4}/\mathrm{DR}_{B,4}/\mathrm{DR}_{C,4}$	0 / 0 / 0	0 / 0 / 0
$F^{\max}_{A,1}/F^{\max}_{B,1}/F^{\max}_{C,1}$	-1.528 / -0.193 / **12.479**	0.645 / -0.923 / **4.149**

same sign, as follows: $\{\mathrm{DR}_{C,1}, P^{\mathrm{d,max}}_{C,1}, F^{\max}_{C,1}, \widehat{P}^{\mathrm{solar}}_{C,1,11\sim16}\}$, $\{P^{\mathrm{d,min}}_{C,1}, P^{\mathrm{c,min}}_{C,1}\}$, and $\{P^{\mathrm{c,max}}_{C,1}, \widehat{P}^{\mathrm{solar}}_{C,1,1\sim10}, \widehat{P}^{\mathrm{solar}}_{C,1,17\sim24}\}$. This grouping property enables system operators to rapidly predict the direction of the DSSE solution to the HEMS data change. We can also list the data in the decreasing order of the absolute sensitivity value, as follows: $\mathrm{DR}_{C,1} > \widehat{P}^{\mathrm{solar}}_{C,1,16} > P^{\mathrm{d,max}}_{C,1} > \widehat{P}^{\mathrm{solar}}_{C,1,15} > P^{\mathrm{d,min}}_{C,1} > \widehat{P}^{\mathrm{solar}}_{C,1,14} > \widehat{P}^{\mathrm{solar}}_{C,1,13} > \widehat{P}^{\mathrm{solar}}_{C,1,11} > F^{\max}_{C,1} = \widehat{P}^{\mathrm{solar}}_{C,1,12} > P^{\mathrm{c,min}}_{C,1} > P^{\mathrm{c,max}}_{C,1} = \widehat{P}^{\mathrm{solar}}_{C,1,1\sim10} = \widehat{P}^{\mathrm{solar}}_{C,1,17\sim24}$. It should be noted that among these data only the $\mathrm{DR}_{C,1}$ can be frequently changed by the system operators to reduce the peak demand. Therefore, a robust DR signal that protects against data corruption needs to be designed to maintain the correct DSSE solution.

Alternatively, the sensitivities of the estimated objective function J (1/puW) to the (G1) data are provided in Table 4. The order of the data impact on J is the same as that of the data impact on the DSSE estimation solution. It is noted that the value of J is used for bad data detection for which the Chi-squares test is used: bad data are suspected if J is larger than some threshold; otherwise bad data are nonexistent. The sensitivity results from Table 4 could help the system operators to prioritize the HEMS data that exert the most significant impact on the performance of bad data detection. From a cybersecurity perspective, these sensitivities with positive or negative signs may be used to identify the following two types of data attacks: (i) the deletion of normal data ($\partial J/\partial \mathbf{a} > 0$); and (ii) the bypass of bad data detection ($\partial J/\partial \mathbf{a} < 0$).

Table. 5 compares the sensitivities of $\widehat{\theta}_{6,C}$ and $\widehat{V}_{6,C}$ at 3 P.M. to $F^{\max}_{p,1}$ and DR for all consumers. As expected,the results from this table show the localized effect of the HEMS data change where $\widehat{\theta}_{6,C}$ and $\widehat{V}_{6,C}$ are more affected by change in the HEMS data for phase C than for phases A and B. In Table. 5, the order of the absolute sensitivity value for all three phases is as follows: $F^{\max}_1 > \mathrm{DR}_1 = \mathrm{DR}_2 = \mathrm{DR}_3 > \mathrm{DR}_4$. Through the comparison of the results between Table. 4 and Table. 5, we observe that the most influential data regarding the sensitivity vary with different HEMS scheduling time: $\mathrm{DR}_{C,1}$ in Table. 4 (11 A.M.) and $F^{\max}_{C,1}$ in Table. 5 (3 P.M.). Similar to Case 1, the sensitivities in Table. 5 corresponding to the HEMS data for phase C are categorized into three groups, each of which has the sensitivity of the same sign but different magnitudes, as follows: $\{F^{\max}_{C,1}, \mathrm{DR}_{C,3}\}$, $\{\mathrm{DR}_{C,1}, \mathrm{DR}_{C,2}\}$ and $\{\mathrm{DR}_{C,4}\}$. It is noted that $\partial\widehat{V}_{6,C}/\partial\mathrm{DR}_{C,1}$ and $\partial\widehat{V}_{6,C}/\partial\mathrm{DR}_{C,2}$ are negative. This is because an increase of $\mathrm{DR}_{C,1}$ and $\mathrm{DR}_{C,2}$ leads to an increase of $P^{\mathrm{net}}_{C,1,15}$ and $P^{\mathrm{net}}_{C,2,15}$, subsequently resulting in a drop of the voltage magnitude at 3 P.M. Alternatively, the sensitivities to the $\mathrm{DR}_{C,3}$ and the $F^{\max}_{C,1}$ at 3 P.M. are positive, because an increase of these data leads to a rise of the voltage magnitude through a decrease of the $P^{\mathrm{net}}_{C,3,15}$ and $F_{C,1,15}$. Lastly, the sensitivity to $\mathrm{DR}_{C,4}$ is zero because $P^{\mathrm{net}}_{C,4,t}$ is not binding at any scheduling time slot.

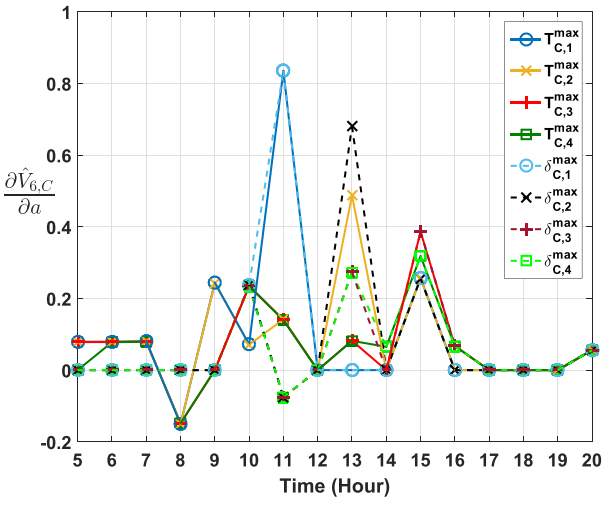

FIGURE 6. Sensitivities of the bus voltage magnitude estimates at bus 6 for phase C to the change in the HEMS (G2) data for four consumers at phase C (Case 2).

2) CASE 2: SENSITIVITY ANALYSIS FOR (G2) DATA CHANGE

In Case 2, the sensitivity of the DSSE to (G2) data for four consumers's thermal comfort levels is quantified. Fig. 6 shows the sensitivities of $\widehat{V}_{6,C}$ (puV/°C) to the change in

two different data, $T^{\max}_{C,u}$ and $\delta^{\max}_{C,u}$ in $t \in$ [5A.M., 8P.M.]. In the maximum value of the absolute sensitivity to these data, the sensitivity order is listed as follows: $T^{\max}_{C,1}(\delta^{\max}_{C,1}) > T^{\max}_{C,2}(\delta^{\max}_{C,2}) > T^{\max}_{C,3}(\delta^{\max}_{C,3}) > T^{\max}_{C,4}(\delta^{\max}_{C,4})$. This result is natural because the consumer's preferred comfortable temperature range becomes narrower from consumer 1 to 4 in the increasing order of the temperature range. In addition, the TOU rate affects the sensitivity of the DSSE to $T^{\max}_{C,u}$ and $\delta^{\max}_{u}$. For example, for all consumers, the sensitivity of $\delta^{\max}_{u}$ is zero in $t \in$ [5A.M., 9A.M.] and $t \in$ [5P.M., 8P.M.] when the TOU rate is inexpensive. However, when the TOU rate suddenly increases at 10 A.M. and 1 P.M., the sensitivity to $\delta^{\max}_{C,u}$ becomes greater than to $T^{\max}_{C,u}$. At the other scheduling time slots, sensitivities associated with both data are the same. Also, from Fig. 6, $\partial \widehat{V}_{6,C}/\partial T^{\max}_{C,u}$ and $\partial \widehat{V}_{6,C}/\partial \delta^{\max}_{C,u}$ are generally positive. This is consistent with our expectation that an increasing of the $T^{\max}_{C,u}$ and the $\delta^{\max}_{C,u}$ would reduce the net power consumption of each consumer, which in turn leads to a rise of the voltage magnitude.

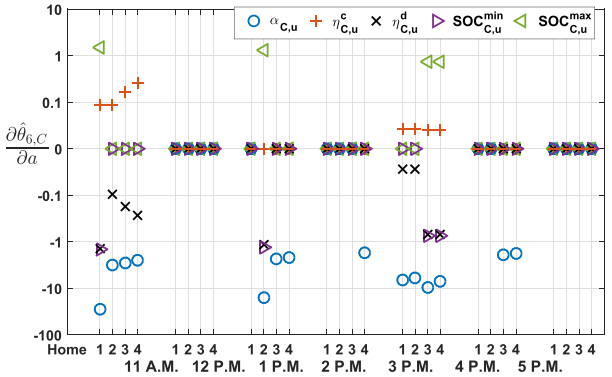

FIGURE 7. Sensitivities of the bus voltage angle estimates at bus 6 for phase C to the change in the HEMS (G3) data for four consumers at phase *C* (Case 3).

3) CASE 3: SENSITIVITY ANALYSIS FOR (G3) DATA CHANGE

In Case 3, the impact of the (G3) data on the $\widehat{\theta}_{6,C}$ from the DSSE in the $t \in$ [11A.M., 5P.M.] is investigated. From Fig. 7, the order of the (G3) data with the absolute on-average sensitivity value can be listed, as follows: $\alpha_{A,u} > \eta^{d}_{A,u} > SOC^{max}_{A,u} = SOC^{min}_{A,u} > \eta^{c}_{A,u}$. It is conjectured from this result that the data associated with the air conditioner impacts the DSSE more than the ESS. From this figure, the time slots are also compared when the change of data of each consumer exerts a significant impact on the DSSE. For example, the sensitivities that are associated with the comfortable data for consumers 1 and 2 are greater than those for consumers 3 and 4 at 11 A.M. and 1 P.M., respectively. Alternatively, for consumers 3 and 4, the sensitivities are greater than those for consumers 1 and 2 at 3 P.M. In addition, the sensitivities at 12 P.M. and 5 P.M. are zero, and this is due to the fact that $L_{6,A}$ is binding at the $F^{\max}_{A,1}$ at 12 P.M. and 5 P.M. so that the change is only regarding the $F^{\max}_{A,1}$ influence on the calculation of the $L_{6,A}$, and subsequently the sensitivity of the DSSE. We note 3 P.M. in Case 3. In general, when $P^{net}_{A,1,15} \sim P^{net}_{A,3,15}$ are bounded to the DR constraint, their sensitivities to the other HEMS data change become zero. However, as shown in the figure, the sensitivity values of HEMS data for household 1∼3 are not zero at 3 P.M. due to the line flow constraint that represents the capacity of total power consumption for household 1∼4. If the flow is binding at a flow constraint, net power consumption can be affected by the HEMS data for the other households. At 3 P.M., HEMS data change for household 1∼3 affect only $P^{net}_{A,4,15}$ without having impact on their own net power consumptions. Due to this reason, the sensitivities of both the aggregated load at 3 P.M. to the HEMS data for household 1∼3 and the corresponding bus voltage angle estimates have non-zero values.

TABLE 6. Performance of the proposed sensitivity analysis framework.

HEMS Data	Δa	$\text{AAD}^{\widehat{\mathbf{x}}}$	AD^{J}
$F^{\max}_{C,1}$	10KW	4.74×10^{-6}	5.02×10^{-8}
$\widehat{P}^{solar}_{C,1,15}$	5KW	6.38×10^{-6}	6.97×10^{-8}
$T^{\max}_{C,1}$	0.5°C	8.82×10^{-6}	1.01×10^{-7}
$\eta^{c}_{C,1}$	0.1	9.2×10^{-7}	2.23×10^{-8}

In addition, the performance of the proposed sensitivity analysis framework is evaluated in terms of average absolute deviation (AAD) and absolute deviation (AD):

$$\text{AAD}^{\widehat{\mathbf{x}}} = \frac{1}{3N_B}\sum_{i=1}^{N_B}\sum_{p=a,b,c}\left|\Delta\hat{x}^{(r)}_{i,p}(\mathbf{a}^{\text{cur}},\mathbf{a}^{\text{new}}) - \Delta\hat{x}^{(a)}_{i,p}(\Delta\mathbf{a})\right|, \tag{37}$$

$$\text{AD}^{J} = \left|\Delta J^{(r)}(\mathbf{a}^{\text{cur}},\mathbf{a}^{\text{new}}) - \Delta J^{(a)}(\Delta\mathbf{a})\right| \tag{38}$$

where

$$\Delta\hat{x}^{(r)}_{i,p}(\mathbf{a}^{\text{cur}},\mathbf{a}^{\text{new}}) = \hat{x}^{(r)}_{i,p}(\mathbf{a}^{\text{cur}}) - \hat{x}^{(r)}_{i,p}(\mathbf{a}^{\text{new}}), \tag{39}$$

$$\Delta\hat{x}^{(a)}_{i,p}(\Delta\mathbf{a}) = \mathbf{S}^{\widehat{\mathbf{x}}}\Delta\mathbf{a}, \tag{40}$$

$$\Delta J^{(r)}(\mathbf{a}^{\text{cur}},\mathbf{a}^{\text{new}}) = J^{(r)}(\mathbf{a}^{\text{cur}}) - J^{(r)}(\mathbf{a}^{\text{new}}), \tag{41}$$

$$\Delta J^{(a)}(\Delta\mathbf{a}) = \mathbf{S}^{J}\Delta\mathbf{a}. \tag{42}$$

Equations (37) and (38) represent the formulas of AAD and AD for state estimate and objective function, respectively. In (39), $\Delta\hat{x}^{(r)}_{i,p}(\mathbf{a}^{\text{cur}},\mathbf{a}^{\text{new}})$ represents the reference value, which illustrates the difference between two DSSE estimation solutions with current HEMS data ($\mathbf{a}^{\text{cur}}$) and new HEMS data ($\mathbf{a}^{\text{new}}$). In this paper, (39) is defined as an existing perturbation method-based equation. On the other hand, in (40), $\Delta\hat{x}^{(a)}_{i,p}(\Delta\mathbf{a})$ indicates the analytical value of the varying estimation solution subject to the HEMS data change ($\Delta\mathbf{a}$), which can be calculated using our proposed sensitivity matrix $\mathbf{S}^{\widehat{\mathbf{x}}}$. Our proposed analytical method is based on (40). Equations (41) and (42) for AD^{J} are also defined similar to (39) and (40). Table 6 shows the results of $\text{AAD}^{\widehat{\mathbf{x}}}$ and AD^{J} when data F_1 and $T^{\max}_{1}$ change. We observe from this table that the solutions from the existing perturbation method are almost consistent with those from the proposed analytical method.

Finally, the meaningful observations from simulation studies of the proposed sensitivity framework can be summarized as follows.

- *Impact of the HEMS data on the DSSE sensitivity under different SCADA measurement redundancy:* decreased SCADA measurement redundancy leads to stronger non-localized effect of the HEMS data on the DSSE performance where variations in the HEMS data at bus i for phase p can be influential to the DSSE solution at the other buses and phases. In the unexpected situation, the proposed sensitivity framework helps system operators to accurately predict which DSSE solution can be affected much more significantly due to the HEMS data changes.
- *Fast assessment of the DSSE sensitivity in response to changes in various types of the HEMS data:* according to the sign and magnitude of the calculated sensitivities, the different types of the HEMS data can be grouped and prioritized. The results are used to quickly identify the most influential HEMS data as well as the direction of the change in the DSSE solution subject to the HEMS data change. Furthermore, the sensitivities to the HEMS data at different scheduling time are compared, and the most affecting HEMS scheduling time to DSSE can be predicted rapidly.

V. CONCLUSIONS

In this paper, an analytical framework is presented for the quantification of the sensitivity of the three phase DSSE in the MV network with respect to changes of the various types of HEMS data in the LV network. The two following sensitivity matrices are constructed: The first comprises a DSSE sensitivity to any SCADA measurement, and the second comprises a sensitivity of the aggregate scheduled load from the HEMS to the HEMS data. Given that the aggregate scheduled load is equal to the SCADA real power injection measurement, a matrix that combines these two matrices in the multiplication form provides the sensitivity information regarding the extent that the DSSE solution (i.e., the estimated bus voltage magnitude/phase angle and objective function) varies when it is subjected to changes of the HEMS data, such as the DR signal, the operation parameters of the appliances, and the consumer preferred indoor temperature. This is the first study to investigate the sensitivity of DSSE subject to the HEMS data changes in the unified sensitivity framework considering the entire MV/LV distribution network.

The sensitivity results from the simulation study could be used as follows: 1) HEMS-data grouping/listing with different sensitivity values, and 2) a segmentation of the LV network into the most- and least-influential residential areas on the DSSE while the HEMS data change. Furthermore, these results may provide guidelines for the design of the DR signal and the development of DSSE and HEMS algorithms that are robust to attacker data manipulation.

APPENDIX A
PERTURBATION SUBMATRICES FOR HEMS

In this appendix, $\mathbf{1}_{(k\times l)}$ and $\mathbf{0}_{(k\times l)}$ are the $k \times l$ matrices with all ones and all zeros, respectively. $\mathbf{I}_k$ is the $k \times k$ identity matrix. N_t is the number of time slots and N_u is the number of smart households that are in same phase. The submatrices in (32) are expressed as follows:

A. THE SUBMATRICES IN THE LEFT-HAND SIDE OF (32)

$$\mathbf{M}_1 = \begin{bmatrix} [\pi_t]_{(1\times N_u N_t)} & \mathbf{0}_{(1\times N_u N_t)} & \mathbf{0}_{(1\times N_u N_t)} \end{bmatrix},$$
$$\mathbf{M}_2 = \begin{bmatrix} \mathbf{0}_{(1\times N_u N_t)} & [\epsilon_u]_{(1\times N_u N_t)} & \mathbf{0}_{(1\times N_u N_t)} \end{bmatrix},$$
$$\boldsymbol{\Upsilon} = \begin{bmatrix} -\mathbf{I}_{N_t} \cdots -\mathbf{I}_{N_t} & \mathbf{0}_{(N_t\times N_u N_t)} & \mathbf{I}_{N_t} \\ \mathbf{I}_{N_u N_t} & \mathbf{0}_{(N_u N_t\times N_u N_t)} & \mathbf{0}_{(N_u N_t\times N_t)} \end{bmatrix}.$$

B. THE SUBMATRICES IN THE RIGHT-HAND SIDE OF (32)

$$\boldsymbol{\Lambda}_1 = \begin{bmatrix} [\sum_{u\in\mathcal{U}} P^{\text{net}}_{u,t}]_{(1\times N_t)} & \sum_{t\in\mathcal{T}} [\delta_{u,t}]_{(1\times N_u)} & \mathbf{0}_{(1\times N_u)} \end{bmatrix},$$
$$\boldsymbol{\Lambda}_2 = \begin{bmatrix} \boldsymbol{\Phi}_1 & \mathbf{0}_{(N_u N_t\times N_u)} & \mathbf{0}_{(N_u N_t\times N_u)} \\ \mathbf{0}_{(N_u N_t\times N_t)} & \boldsymbol{\Phi}_2 & \mathbf{0}_{(N_u N_t\times N_u)} \\ \mathbf{0}_{(N_u N_t\times N_t)} & \mathbf{0}_{(N_u N_t\times N_u)} & \mathbf{0}_{(N_u N_t\times N_u)} \end{bmatrix},$$
$$\boldsymbol{\Lambda}_3 = \begin{bmatrix} \mathbf{0}_{(N_t\times N_t)} & \mathbf{0}_{(N_t\times N_u)} & \mathbf{0}_{(N_t\times N_u)} \\ \mathbf{0}_{(N_u N_t\times N_t)} & \mathbf{0}_{(N_u N_t\times N_u)} & \boldsymbol{\Phi}_3 \end{bmatrix},$$

where

$$\boldsymbol{\Phi}_1 = \begin{bmatrix} -\mathbf{I}_{N_t} \cdots -\mathbf{I}_{N_t} \end{bmatrix}^T_{(N_t\times N_u N_t)},$$
$$\boldsymbol{\Phi}_2 = \begin{bmatrix} \text{Diag}^{(N_u)}(\mathbf{1})^T_{N_t\times 1} \end{bmatrix}^T_{(N_u\times N_u N_t)},$$
$$\boldsymbol{\Phi}_3 = \begin{bmatrix} \text{Diag}^{(N_u)}([\mathbf{0}\ \mathbf{1}_{(1\times \mathbf{D_u})}\ \mathbf{0}])_{N_t\times 1} \end{bmatrix}^T_{(N_u\times N_u N_t)}.$$

Here, $\text{Diag}^{(A)}(\mathbf{B})$ is a block diagonal matrix with A blocks of the matrix $\mathbf{B}$.

APPENDIX B
PERTURBATION SUBMATRICES FOR DSSE

In addition to notations in Appendix A, $|S|$ represents the cardinality of a set S (i.e., the number of elements in S). N_B is the number of buses on distribution system. The submatrices in (34) are written as follows:

A. THE SUBMATRICES IN THE LEFT-HAND SIDE OF (34)

$$\mathbf{M} = \begin{bmatrix} \mathbf{0}_{(1\times 6N_B)} & [-2\omega^P_{i,p}(P^z_{i,p} - P_{i,p})]_{(1\times|\mathcal{B}_{P_I}|)} \end{bmatrix}$$
$$\boldsymbol{\Upsilon}_1 = = \boldsymbol{\Pi}_1 + \boldsymbol{\Pi}_2$$

where

$$\boldsymbol{\Pi}_1 = \begin{bmatrix} \mathbf{0}_{(3N_B\times 3N_B)} & \mathbf{0} & \mathbf{0} \\ \mathbf{0} & \mathbf{0}_{(3N_B\times 3N_B)} & \mathbf{0} \\ \mathbf{0} & \mathbf{0} & \text{Diag}(2\omega^P_{i,p})_{(|\mathcal{B}_{P_I}|\times|\mathcal{B}_{P_I}|)} \end{bmatrix},$$

$$\boldsymbol{\Pi}_2 = \begin{bmatrix} \dfrac{\partial^2\mathbf{P}}{\partial\mathbf{V}\partial\mathbf{V}} & \dfrac{\partial^2\mathbf{P}}{\partial\mathbf{V}\partial\boldsymbol{\theta}} & \mathbf{0}_{(3N_B\times|\mathcal{B}_{P_I}|)} \\ \dfrac{\partial^2\mathbf{P}}{\partial\boldsymbol{\theta}\partial\mathbf{V}} & \dfrac{\partial^2\mathbf{P}}{\partial\boldsymbol{\theta}\partial\boldsymbol{\theta}} & \mathbf{0}_{(3N_B\times|\mathcal{B}_{P_I}|)} \\ \mathbf{0}_{(|\mathcal{B}_{P_I}|\times 3N_B)} & \mathbf{0}_{(|\mathcal{B}_{P_I}|\times 3N_B)} & \mathbf{0}_{(|\mathcal{B}_{P_I}|\times|\mathcal{B}_{P_I}|)} \end{bmatrix},$$

Here, the matrix $\mathbf{\Pi}_2$ is called as the Hessian matrix for DSSE, which is the symmetric matrix. The following matrix $\mathbf{\Upsilon}_2$ is a derivative matrix of any constraint with respect to any variable for DSSE, which is similar to the Jacobian matrix:

$$\mathbf{\Upsilon}_2 = \begin{bmatrix} -\dfrac{\partial \mathbf{P}}{\partial \mathbf{V}}_{(3N_B \times |\mathcal{B}_{P_I}|)} \\ -\dfrac{\partial \mathbf{P}}{\partial \boldsymbol{\theta}}_{(3N_B \times |\mathcal{B}_{P_I}|)} \\ \mathbf{I}_{|\mathcal{B}_{P_I}|} \end{bmatrix}.$$

B. THE SUBMATRICES IN THE RIGHT-HAND SIDE OF (34)

$$\mathbf{\Lambda} = \begin{bmatrix} \mathbf{0}_{(6N_B \times |\mathcal{B}_{P_I}|)} \\ \text{Diag}(-2\omega_{k,p}^{P})_{(|\mathcal{B}_{P_I}| \times |\mathcal{B}_{P_I}|)} \end{bmatrix}.$$

REFERENCES

[1] A. P. S. Meliopoulos, E. Polymeneas, Z. Tan, R. Huang, and D. Zhao, "Advanced distribution management system," *IEEE Trans. Smart Grid*, vol. 4, no. 4, pp. 2109–2117, Dec. 2013.
[2] M. Pipattanasomporn, M. Kuzlu, and S. Rahman, "An algorithm for intelligent home energy management and demand response analysis," *IEEE Trans. Smart Grid*, vol. 3, no. 4, pp. 2166–2173, Dec. 2012.
[3] X. Chen, T. Wei, and S. Hu, "Uncertainty-aware household appliance scheduling considering dynamic electricity pricing in smart home," *IEEE Trans. Smart Grid*, vol. 4, no. 2, pp. 932–941, Jun. 2013.
[4] Z. Yu, L. Jia, M. C. Murphy-Hoye, A. Pratt, and L. Tong, "Modeling and stochastic control for home energy management," *IEEE Trans. Smart Grid.*, vol. 4, no. 4, pp. 2244–2255, Dec. 2013.
[5] M. D. Somma, G. Graditi, E. Heydarian-Forushani, M. Shafie-Khah, and P. Siano, "Stochastic optimal scheduling of distributed energy resources with renewables considering economic and environmental aspects," *Renew. Energy.*, vol. 116, pp. 272–287, Feb. 2018.
[6] M. Shafie-khah and P. Siano, "A stochastic home energy management system considering satisfaction cost and response fatigue," *IEEE Trans. Ind. Informat.*, vol. 14, no. 2, pp. 629–638, Feb. 2018, doi: 10.1109/TII.2017.2728803.
[7] D. T. Nguyen and L. B. Le, "Joint optimization of electric vehicle and home energy scheduling considering user comfort preference," *IEEE Trans. Smart Grid*, vol. 5, no. 1, pp. 188–199, Jan. 2014.
[8] P. Palensky and D. Dietrich, "Demand side management: Demand response, intelligent energy systems, and smart loads," *IEEE Trans. Ind. Informat.*, vol. 7, no. 3, pp. 381–388, Aug. 2011.
[9] O. Erdinc, N. G. Paterakis, T. D. P. Mendes, A. G. Bakirtzis, and J. P. S. Catalão, "Smart household operation considering bi-directional EV and ESS utilization by real-time pricing-based DR," *IEEE Trans. Smart Grid*, vol. 6, no. 3, pp. 1281–1291, May 2015.
[10] N. G. Paterakis, O. Erdinç, I. N. Pappi, A. G. Bakirtzis, and J. P. S. Catalão, "Coordinated operation of a neighborhood of smart households comprising electric vehicles, energy storage and distributed generation," *IEEE Trans. Smart Grid.*, vol. 7, no. 6, pp. 2736–2747, Nov. 2016.
[11] Y. Huang, L. Wang, W. Guo, Q. Kang, and Q. Wu, "Chance constrained optimization in a home energy management system," *IEEE Trans. Smart Grid.*, vol. 9, no. 1, pp. 252–260, Jan. 2018.
[12] Y. W. Law, T. Alpcan, V. C. S. Lee, A. Lo, S. Marusic, and M. Palaniswami, "Demand response architectures and load management algorithms for energy-efficient power grids: A survey," in *Proc. 7th Int. Conf. Knowl, Inf. Creativity Support Syst. (KICSS)*, Nov. 2012, pp. 134–141.
[13] A. Saha, S. Rahman, M. Pipattanasomporn, and M. Kuzlu, "On security of a home energy management system," in *Proc. IEEE PES Innov. Smart Grid Technol. Conf. Eur. (ISGT-Eur.)*, Oct. 2014, pp. 1–5.
[14] M. E. Baran and A. W. Kelley, "State estimation for real-time monitoring of distribution systems," *IEEE Trans. Power Syst.*, vol. 9, no. 3, pp. 1601–1609, Aug. 1994.
[15] C. N. Lu, J. H. Teng, and W.-H. E. Liu, "Distribution system state estimation," *IEEE Trans. Power Syst.*, vol. 10, no. 1, pp. 229–240, Feb. 1995.
[16] D. A. Haughton and G. T. Heydt, "A linear state estimation formulation for smart distribution systems," *IEEE Trans. Power Syst.*, vol. 28, no. 2, pp. 1187–1195, May 2013.
[17] J. Liu, F. Ponci, A. Monti, C. Muscas, P. A. Pegoraro, and S. Sulis, "Optimal meter placement for robust measurement systems in active distribution grids," *IEEE Trans. Instrum. Meas.*, vol. 63, no. 5, pp. 1096–1105, May 2014.
[18] R. Singh, B. C. Pal, R. A. Jabr, and R. B. Vinter, "Meter placement for distribution system state estimation: An ordinal optimization approach," *IEEE Trans. Power Syst.*, vol. 26, no. 4, pp. 2328–2335, Nov. 2011.
[19] E. Manitsas, R. Singh, B. C. Pal, and G. Strbac, "Distribution system state estimation using an artificial neural network approach for pseudo measurement modeling," *IEEE Trans. Power Syst.*, vol. 27, no. 4, pp. 1888–1896, Nov. 2012.
[20] F. Shabaninia, M. Vaziri, S. Vadhva, and J. Vaziri, "A novel state estimation formulation for distribution grids with renewable energy sources," in *Proc. IEEE Power Energy Soc. General Meeting*, San Diego, CA, USA, Jul. 2012, pp. 1–5.
[21] P. Rousseaux, J.-F. Toubeau, Z. De Grève, F. Vallée, M. Glavic, and T. Van Cutsem, "A new formulation of state estimation in distribution systems including demand and generation states," in *Proc. IEEE Eindhoven PowerTech*, Eindhoven, The Netherlands, Jun. 2015, pp. 1–6.
[22] H. Wang, W. Zhang, and Y. Liu, "A robust measurement placement method for active distribution system state estimation considering network reconfiguration," *IEEE Trans. Smart Grid.*, to be published, doi: 10.1109/TSG.2016.2606700.
[23] Y. Yao, X. Liu, and Z. Li, "Robust measurement placement for distribution system state estimation," *IEEE Trans. Sustain. Energy*, to be published, doi: 10.1109/TSTE.2017.2775862.
[24] M. Pau, F. Ponci, A. Monti, S. Sulis, C. Muscas, and P. A. Pegoraro, "An efficient and accurate solution for distribution system state estimation with multiarea architecture," *IEEE Trans. Instrum. Meas.*, vol. 66, no. 5, pp. 910–919, May 2017.
[25] A. Primadianto and C.-N. Lu, "A review on distribution system state estimation," *IEEE Trans. Power Syst.*, vol. 32, no. 5, pp. 3875–3883, Sep. 2017, doi: 10.1109/TPWRS.2016.2632156.
[26] E. Castillo, A. J. Conejo, C. Castillo, R. Mínguez, and D. Ortigosa, "Perturbation approach to sensibility analysis in mathematical programming," *J. Optim. Theory Appl.*, vol. 128, no. 1, pp. 49–74, Jan. 2006.
[27] A. J. Conejo, E. Castillo, R. Mínguez, and F. Milano, "Locational marginal price sensitivities," *IEEE Trans. Power Syst.*, vol. 20, no. 4, pp. 2026–2033, Nov. 2005.
[28] R. Minguez and A. J. Conejo, "State estimation sensitivity analysis," *IEEE Trans. Power Syst.*, vol. 22, no. 3, pp. 1080–1091, Aug. 2007.
[29] D.-H. Choi and L. Xie, "Sensitivity analysis of real-time locational marginal price to SCADA sensor data corruption," *IEEE Trans. Power Syst.*, vol. 29, no. 3, pp. 1110–1120, May 2014.
[30] D.-H. Choi and L. Xie, "A framework for sensitivity analysis of data errors on home energy management system," *Energy*, vol. 117, no. 1, pp. 165–175, Dec. 2016.
[31] A. Molin, H. Sandberg, and M. Johansson, "A study on the sensitivity matrix in power system state estimation by using sparse principal component analysis," in *Proc. IEEE 55th Conf. Decision Control (CDC)*, Las Vegas, NV, USA, Dec. 2016, pp. 1529–1535.
[32] M. Pau, P. A. Pegoraro, and S. Sulis, "Performance of three-phase WLS distribution system state estimation approaches," in *Proc. IEEE Int. Workshop Appl. Meas. Power Syst. (AMPS)*, Sep. 2015, pp. 138–143.
[33] W. H. Kersting, "Radial distribution test feeders," *IEEE Trans. Power Syst.*, vol. 6, no. 3, pp. 975–985, Aug. 1991.

JEONG-WON KANG (S'17) received the B.S. degree in electrical and electronics engineering from Chung-Ang University, Seoul, South Korea, in 2015, where he is currently pursuing the M.S. degree. His current research interests include power system state estimation and cybersecurity of smart grid.

LE XIE (S'05–M'10–SM'17) received the B.E. degree in electrical engineering from Tsinghua University, Beijing, China, in 2004, the M.Sc. degree in engineering sciences from Harvard University, Cambridge, MA, USA, in 2005, and the Ph.D. degree in electrical and computer engineering from Carnegie Mellon University, Pittsburgh, PA, USA, in 2009. His industrial experience includes an internship with ISO-New England in 2006 and Edison Mission Energy Marketing and Trading in 2007. He is currently an Associate Professor with the Department of Electrical and Computer Engineering, Texas A&M University, College Station, TX, USA. His research interests include modeling and control of large-scale complex systems, smart grid application with renewable energy resources, and electricity markets.

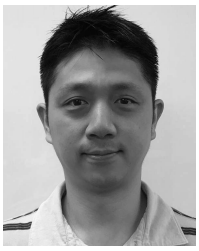

DAE-HYUN CHOI (S'10–M'17) received the B.S. degree in electrical engineering from Korea University, Seoul, South Korea, in 2002, and the M.Sc. degree and the Ph.D. degree in electrical and computer engineering from Texas A&M University, College Station, TX, USA, in 2008 and 2014, respectively. From 2002 to 2006, he was a Researcher with Korea Telecom (KT), Seoul, where he was involved in designing and implementing home network systems. From 2014 to 2015, he was a Senior Researcher with LG Electronics, Seoul, where he developed home energy management systems. He is currently an Assistant Professor with the School of Electrical and Electronics Engineering, Chung-Ang University, Seoul. His research interests include power system state estimation, electricity markets, the cyber-physical security of smart grids, and the theory and application of cyber-physical energy systems. He received the Best Paper Award at the 2012 IEEE Third International Conference on Smart Grid Communications, Tainan, Taiwan.